

## Electronic Supplementary Information

### Integrating a zwitterionic peptide with a two-photoelectrode system for an advanced photoelectrochemical immunosensing platform

Yaqun Xu<sup>a</sup>, Huimin Chen<sup>a</sup>, Zhi-Ling Song<sup>a</sup>, Gao-Chao Fan<sup>\*ab</sup>, and Xiliang Luo<sup>\*a</sup>

<sup>a</sup> *Shandong Key Laboratory of Biochemical Analysis, College of Chemistry and Molecular Engineering, Qingdao University of Science and Technology, Qingdao 266042, China*

<sup>b</sup> *State Key Laboratory of Chemo/Biosensing and Chemometrics, College of Chemistry and Chemical Engineering, Hunan University, Changsha, Hunan 410082, China*

#### Corresponding Authors

E-mail address: gcfan@qust.edu.cn (G.-C. Fan); xiliangluo@qust.edu.cn (X. Luo)

- Section 1:** Experimental details
- Section 2:** Characterization of Pt nanoparticles
- Section 3:** Concentration estimation of Pt nanoparticles
- Section 4:** Photoelectric behavior of the ZIS/FTO photoanode
- Section 5:** PEC monitoring of the antifouling biocathode
- Section 6:** EIS monitoring of the antifouling biocathode
- Section 7:** Characteristics analysis of the zwitterionic peptide
- Section 8:** Optimization of the immunosensing platform
- Section 9:** Antifouling durability of the sensing platform
- Section 10:** Reproducibility, storage stability, and feasibility
- Section 11:** References

## Section 1: Experimental

**Materials and Reagents.** Fluorine-doped tin oxide (FTO) electrodes (square resistance  $\leq 7 \Omega$ , thickness 500 nm, transmittance  $\geq 80\%$ ) were obtained from Hunan South China Xiangcheng Technology Co., Ltd (China). Zinc sulfate ( $\text{ZnSO}_4 \cdot 7\text{H}_2\text{O}$ ), dimethyl sulphoxide (DMSO), sodium hydroxide (NaOH), sodium borohydride ( $\text{NaBH}_4$ ), chloroplatinic acid ( $\text{H}_2\text{PtCl}_6$ ), sodium citrate, and ascorbic acid (AA) were purchased from Sinopharm Chemical Reagent Co., Ltd. (China). Indium (III) chloride ( $\text{InCl}_3 \cdot 4\text{H}_2\text{O}$ ), thioacetamide (TAA), sulfur (S) powder, and copper (II) chloride ( $\text{CuCl}_2 \cdot 2\text{H}_2\text{O}$ ) were purchased from Aladdin Biochemical Technology Co., Ltd. (China). Carbohydrate antigen 15-3 (CA15-3, Ag), CA15-3 capture antibody (Ab), and carbohydrate antigen 12-5 (CA12-5) was obtained from Beijing Solarbio Science & Technology Co., Ltd. (Beijing, China). Cardiac troponin I (cTnI), human serum albumin (HSA), human immunoglobulin G (HIgG), and  $\alpha$ -fetoprotein (AFP) were purchased from Shanghai Linke Biotechnology Co., Ltd. (China).

The designed zwitterionic peptide was ordered by Bankpeptide biological technology Co., Ltd. (Hefei, China). The peptide sequence was SKSESKSEPPPPC, where E, S, K, P and C represent glutamic acid, serine, lysine, proline, and cysteine, respectively. The molecular structure of the zwitterionic peptide is shown in Fig. S1. Phosphate buffer solution (PBS) with pH 7.4 and concentration of 10 mM served as the solvent of the peptide solution, antibody solution, and antigen solution.

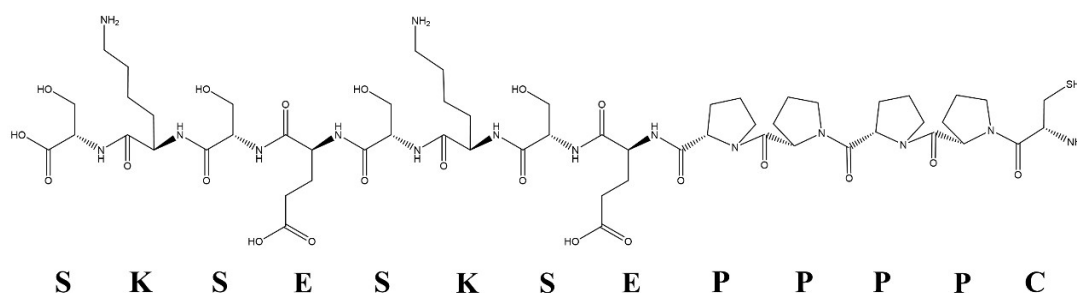


**Fig. S1.** The structure of the designed zwitterionic peptide SKSESKSEPPPPC.

**Apparatus.** PEC measurements were conducted on a Zahner photoelectrochemical workstation (ZAHNER-elektrik GmbH & Co. KG, Germany) with a two-electrode system: a modified Pt/CIS/FTO photocathode with an area of  $0.7 \times 0.7 \text{ cm}^2$  as working electrode, and a ZIS/FTO photoanode itself as counter electrode. Transmission electron microscopy (TEM) was performed with a JEOL-2100 transmission electron microscope (JEOL, Japan). Scanning electron microscope (SEM) images were recorded on a

Hitachi S-4800 scanning electron microscope (Hitachi Co., Japan). X-ray diffraction (XRD) was performed on a Philips X'pert Pro X-ray diffractometer (Cu  $K\alpha$  radiation,  $\lambda=0.15418$  nm, Netherlands). X-ray photoelectron spectroscopy (XPS) pattern was obtained from an ESCALAB 250Xi spectrometer (Thermo Fisher Scientific, UK) with a monochromatic Al  $K\alpha$  X-ray source, and all spectra were calibrated by normalizing the C (1s) peak to the standard value of 284.6 eV. The electrochemical impedance spectroscopy (EIS) was performed on a CHI 760D electrochemical workstation (Shanghai Chenhua Instrument Co. Ltd., China) with a typical three-electrode system in 0.1 M KCl containing 5.0 mM  $K_3[Fe(CN)_6]/K_4[Fe(CN)_6]$  (1:1) mixture as a redox probe, and recorded in the frequency range of 0.01 Hz-100 kHz with an amplitude of 50 mV. Confocal fluorescence imaging was performed using a TCS SP5 confocal laser microscope (Leica, Germany). Zeta potential measurement was carried out on a ZETASIZER Nano-ZS (Malvern, U.K.). The hydrophilicity of electrode surface was tested on a contact angle measuring instrument (JC2000D1 Shanghai Zhongchen Instrument Co., China).

**Fabrication of ZIS/FTO photoanode.** The in-situ growth of ZIS on the FTO electrode was according to a previous method with some modifications,<sup>1</sup> and the synthetic process was outlined in Fig. S2. Typically, 0.0647 g (15 mM) of  $ZnSO_4 \cdot 7H_2O$ , 0.1320 g (30 mM) of  $InCl_3 \cdot 4H_2O$  and 0.0676 g (60 mM) of TAA were added in sequence into 15 mL of deionized water, and kept stirring for 30 min to acquire precursor solution. Subsequently, the clean FTO electrodes were placed into a 25 mL polytetrafluoroethylene liner at an angle about 55°, and then right amount of precursor solution was injected. After the autoclave with digestion liner was sealed and kept at 160 °C for 12 h, a yellow ZIS film was found to grow on the surface of the FTO electrodes. The final ZIS/FTO photoanode was rinsed gently with ethanol and water, and then dried in air naturally.

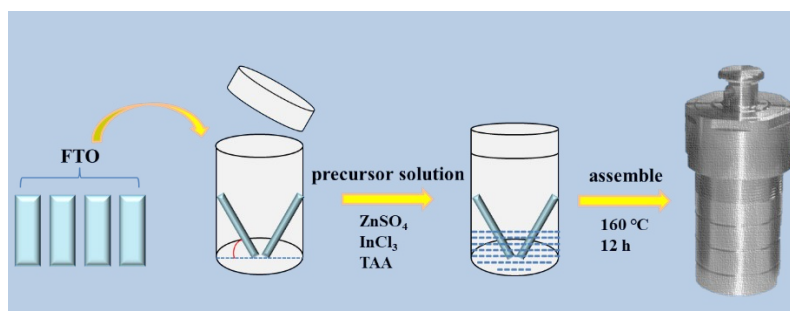


**Fig. S2.** Schematic diagram for the synthetic process of the ZIS/FTO photoanode.

**Synthesis of Pt nanoparticles.** An updated one-pot method was used to obtain Pt nanoparticles.<sup>2</sup> Typically, 9 mg sodium citrate was firstly added into a 45 mL of 0.24 mM  $\text{H}_2\text{PtCl}_6$  aqueous solution under high-speed stirring for 10 min. Then, 5 mL of  $\text{NaBH}_4$  aqueous solution (30 mM) was added dropwise to the above mixed solution, and the color of the solution changed rapidly. After the operations above were finished, a uniform Pt nanoparticle solution was formed in dark condition for continuous stirring of 30 minutes. The stock solution of Pt nanoparticles was stored at 4 °C of a refrigerator and diluted to different concentrations for next used.

**Preparation of Pt/CIS/FTO photocathode.** For preparation of the Pt/CIS/FTO photocathode, CIS thin film was firstly deposited on a FTO electrode by a mature potentiostatic method.<sup>3</sup> Typically, the electrolyte solution was a DMSO water-free deposition solution that dissolved with 4 mM  $\text{CuCl}_2$ , 4 mM  $\text{InCl}_3$  and 12 mM S powder. The electrochemical process lasted for a period of 30 min under a fixed deposition potential of  $E = -1.30 \text{ V vs Hg/Hg}_2\text{Cl}_2$ . After rinsing and drying, the CIS/FTO electrode was obtained and it appeared as a uniform layer of yellow-brown film. For surface modification of Pt, 20  $\mu\text{L}$  of the purified Pt nanoparticle solution with a certain concentration were casted on the CIS/FTO electrode above for electrostatic adsorption. After air-drying at natural temperature, the construction of the Pt/CIS/FTO photocathode was completed.

**Construction of antifouling biointerface.** Typically, 20  $\mu\text{L}$  of CA15-3 capture antibody (Ab) with an optimized concentration was firstly casted on the Pt/CIS/FTO photocathode and incubated at 4 °C of a refrigerator for overnight. After Ab anchoring via  $\text{NH}_2\text{-Pt}$  bond, the modified electrode was rinsed with PBS (10 mM,  $\text{pH}=7.4$ ) and subsequently incubated with 0.2 mg/mL zwitterionic peptide at 4 °C of a refrigerator for 6 h. With zwitterionic peptide anchoring via steady  $\text{S-Pt}$  bond,<sup>4</sup> an antifouling biointerface on the sensing electrode was formed. Toward target antigen (Ag) of CA15-3 detection, only the antifouling sensing electrode was incubated with target Ag at ambient temperature for 1 h, and followed by PBS rinsing. Subsequently, the incubated antifouling biocathode and ZIS/FTO photoanode above were fixed in a transparent vessel for next PEC measurement.

**PEC measurement.** The method of chopped light voltammetry was employed for PEC test without applied potential. PEC determination was operated at ambient temperature in a typical two-electrode

system: an incubated antifouling biocathode as working electrode and a steady ZIS/FTO photoanode as counter electrode; and the electrolyte was PBS (10 mM, pH 7.4) dissolved with 0.1 M ascorbic acid (AA), which played the role of electron donor of the photoanode. A LED lamp with 430 nm emission wavelength and 350 W/m<sup>2</sup> light intensity acted as the irradiation source that shined on both photoanode and antifouling biocathode, and was turned on/off every 10 s.

## Section 2: Characterization of Pt nanoparticles

Fig. S3A shows TEM image of the synthesized Pt nanoparticles, and large number of nanoparticles with clear outlines were dispersed evenly. The inset of Fig. S3A presents typical high-resolution TEM image of a single Pt nanoparticle, and the lattice spacing was measured to be 0.227 nm, which was consistent with the spacing of (111) crystal plane of cubic platinum. From size distribution histogram in Fig. S3B, an average size of 4.3±0.9 nm of the synthesized Pt nanoparticles was acquired. Actually, after stored at 4 °C in a refrigerator for one month, the as-prepared Pt nanoparticles solution still remained uniform brown solution and without sediments, illustrating good water dispersibility and stability.

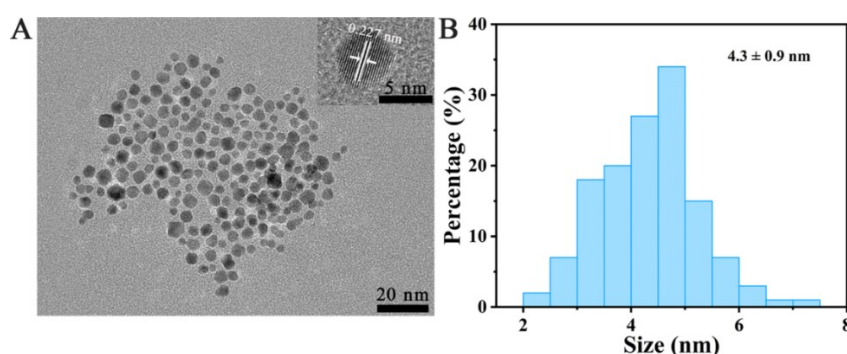


**Fig. S3.** (A) TEM image and (B) size distribution histogram of Pt nanoparticles. Inset in A: high-resolution TEM image of a single Pt nanoparticle.

## Section 3: Concentration estimation of Pt nanoparticles

The concentration of Pt nanoparticles solution can be roughly estimated by the method as below.

As obtained from Fig. S3, the average size ( $d$ ) of the Pt nanoparticles was 4.3 nm. Thus, the volume ( $V_s$ ) of a single Pt nanoparticle can be calculated from the equation (1).

$$V_s = \frac{4}{3}\pi\left(\frac{d}{2}\right)^3 = \frac{4}{3}\pi\left(\frac{4.3}{2}\right)^3 \approx 41.61 \text{ nm}^3$$

Since the density ( $\rho$ ) of Pt at room temperature is  $21.45 \text{ g/cm}^3$ , the mass ( $M_s$ ) of a single Pt nanoparticle can be calculated from the equation (2).

$$M_s = \rho V_s = 21.45 \text{ g/cm}^3 \times 41.61 \text{ nm}^3 \approx 8.9 \times 10^{-19} \text{ g}$$

Then, 1 mL of this sample of purified Pt nanoparticles solution was accurately measured and dried to obtain its total mass ( $M_t$ ). The  $M_t$  was measured to be about 2.6 mg.

The amount of substance ( $n$ ) of Pt nanoparticles in 1 mL solution can be obtained by the equation (3). Thereinto,  $N_A$  stand for Avogadro constant.

$$n = \frac{M_t}{M_s \times N_A} \approx 5.0 \times 10^{-9} \text{ mol}$$

And finally, the concentration ( $c$ ) of the Pt nanoparticles can be obtained from the equation (4).

$$c = \frac{n}{v} = \frac{5.0 \times 10^{-9} \text{ mol}}{1 \text{ mL}} \approx 5.0 \mu\text{M}$$

#### Section 4: Photoelectric behavior of the ZIS/FTO photoanode

To obtain better photoelectric property, the fabrication of the ZIS/FTO photoanode was explored, with a Pt wire as counter electrode. Fig. S4A shows photocurrent output of the ZIS/FTO photoanode with varied concentration of  $\text{ZnSO}_4$  and fixed molar ratio of  $\text{ZnSO}_4/\text{InCl}_3/\text{TAA}$ . As shown, with increase in  $\text{ZnSO}_4$  concentration, the photocurrent output enhanced at beginning and then decreased gradually after reached a peak value corresponding to 15 mM  $\text{ZnSO}_4$ . This was because that ZIS with appropriate thickness could harvest the light energy adequately, but the extra thickness would generate accumulated surface recombination sites to hinder charge transfer. Thus, 15 mM of  $\text{ZnSO}_4$  concentration was used for photoanode fabrication.

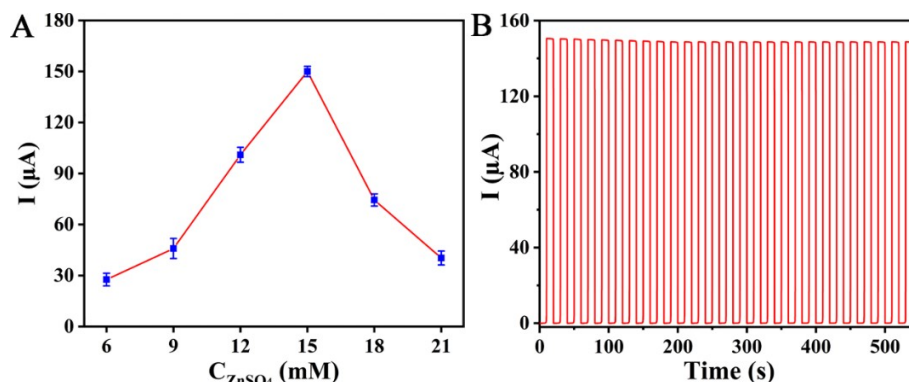


**Fig. S4.** (A) Photocurrent output of the ZIS/FTO photoanode with varied concentration of  $\text{ZnSO}_4$ ; (B) time-varying photocurrent output of the ZIS/FTO photoanode.

Besides, the stability of the ZIS/FTO photoanode was investigated by time-varying photocurrent output. As shown in Fig. S4B, the photocurrent intensity almost had no decay when the ZIS/FTO photoanode continuously suffered from dozens of irradiation cycles, substantiating good photo-chemical stability of the fabricated photoanode.

### Section 5: PEC monitoring of the antifouling biocathode

PEC monitoring was first utilized to inspect stepwise fabrication of the antifouling biocathode, with the ZIS/FTO photoanode as counter electrode, as depicted in Fig. S5. The bare FTO electrode appeared a moderate cathodic current response (curve a). After CIS deposition, a marked increase in the current response was observed (curve b), owing to its efficient visible-light adsorption. After Pt decoration, a further evident enhancement in the current response was obtained (curve c), because of its good electrical conductivity and catalytic ability for  $O_2$  reduction reaction. After Ab immobilization and then zwitterionic peptide anchoring, the current response declined successively (curves d and e), illustrating that their evident steric hindrance had hindered the charge exchange of the system. While the antifouling biocathode was incubated with CA15-3, the current response further declined (curve f), implying that the target molecules were captured by the sensing electrode via the specific immunoreaction between antibody probe and target antigen. The expected result of PEC monitoring demonstrated successful construction of the immunosensing platform.

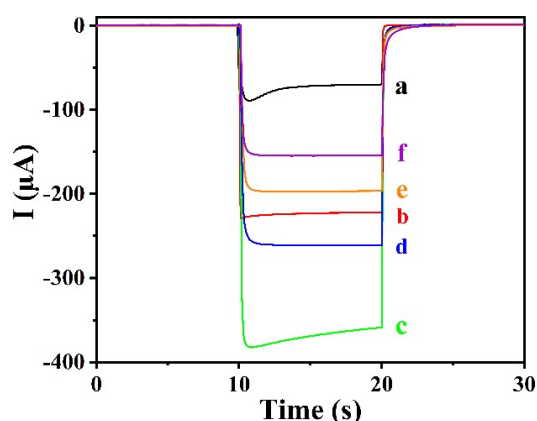


**Fig. S5.** Current responses of the FTO electrode (a), after CIS electrodeposition (b), after Pt decoration (c), after Ab immobilization (d), after zwitterionic peptide anchoring (e), and finally after target CA15-3 incubation (f).

## Section 6: EIS monitoring of the antifouling biocathode

The stepwise building of the antifouling biocathode was inspected further by EIS, as shown in Fig. S6. The semicircle diameter of the spectrum equals the electron transfer resistance ( $R_{et}$ ) during the electrode modification. The bare FTO substrate had a small  $R_{et}$  (curve a). After CIS deposition, the  $R_{et}$  increased moderately (curve b) owing to weak conductivity of the semiconductor CIS. After Pt decoration, the  $R_{et}$  reduced obviously (curve c) because of good electron conductivity of metallic Pt. After Ab immobilization and zwitterionic peptide anchoring, gradually increased  $R_{et}$  was observed (curves d and e) due to insulating property of protein and peptide molecules. After target CA15-3 incubation, the  $R_{et}$  further increased (curve f), implying the formation of the specific immunocomplex between Ab and target CA15-3. The variation trend of EIS supported successful fabrication of the antifouling biocathode.

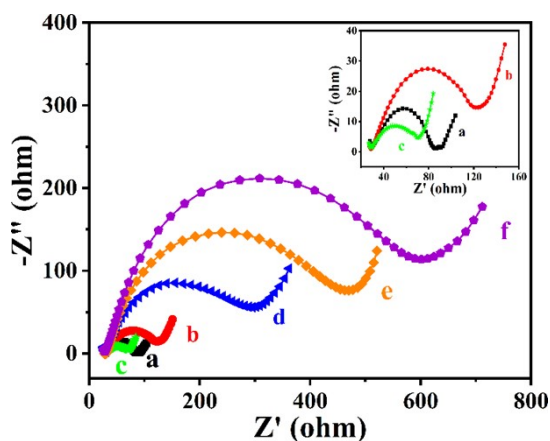
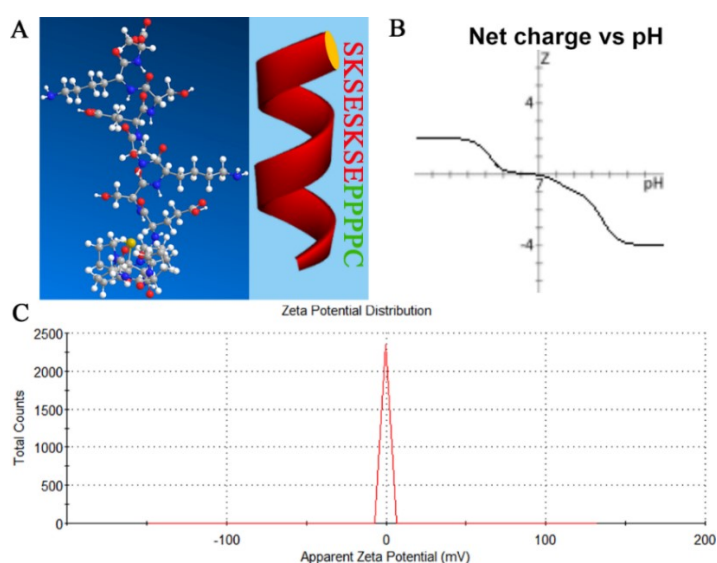


**Fig. S6.** Impedance spectra of the FTO electrode (a), after CIS electrodeposition (b), after Pt decoration (c), after Ab immobilization (d), after zwitterionic peptide anchoring (e), and finally after target CA15-3 incubation (f).

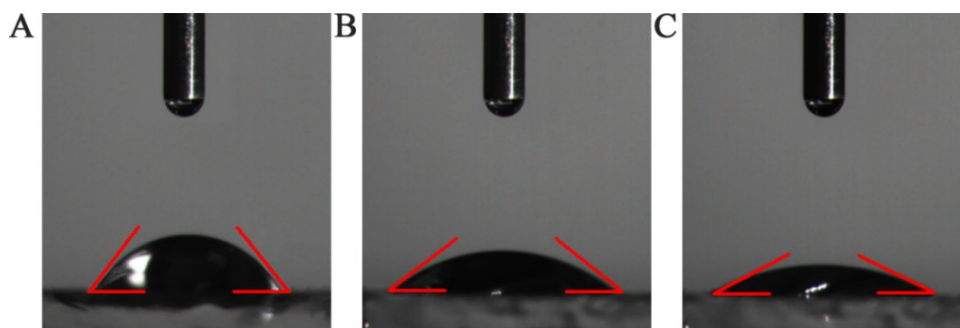
## Section 7: characteristics analysis of the zwitterionic peptide

Fig. S7A shows molecular dynamics simulation diagram of the designed zwitterionic peptide anchored on the electrode surface, and the linear structure of the peptide had a good vertical effect, which was conducive to the formation of interface brush with high density.<sup>5</sup> As noted, electric neutrality and good hydrophilicity are two key factors toward the antifouling nature of the zwitterionic peptide. For electric neutrality: (i) theoretical calculation in Fig. S7B shows that the net charge of the zwitterionic peptide was close to zero under neutral pH condition; (ii) the experimental test in Fig. S7C exhibits that the value of

the zeta potential was approximately 0.0 mV, further indicating electric neutrality of the zwitterionic peptide. The hydrophilicity of the zwitterionic peptide was examined by static water contact angle of the electrode surfaces shown in Fig. S8, and the tested values were listed in Table S1. As observed, the contact angle of the Pt/CIS/FTO photocathode was measured to be 57.40°. With modification of Ab on the photocathode, the contact angle decreased to 37.36°. After further anchoring of the zwitterionic peptide, the contact angle decreased obviously to 22.62°, illustrating good hydrophilicity. The characteristics of electric neutrality and good hydrophilicity of the designed zwitterionic peptide provided a theoretical basis for potential antifouling ability of the immunosensing platform.



**Fig. S7.** (A) Molecular dynamics simulation diagram of the designed zwitterionic peptide; (B) theoretical calculation for the relationship between net charge of the zwitterionic peptide and pH condition; (C) Zeta potential of the zwitterionic peptide at 1.0 mg/mL.



**Fig. S8.** Static water contact angles of the (A) Pt/CIS/FTO, (B) Ab/Pt/CIS/FTO, and (C) ZP/Ab/Pt/CIS/FTO electrode surfaces. (ZP represents zwitterionic peptide).

**Table S1.** Tested values of water contact angles of the Pt/CIS/FTO, Ab/Pt/CIS/FTO, and ZP/Ab/Pt/CIS/FTO electrode surfaces.

Points	Surface contact angle (°)		
	Pt/CIS/FTO	Ab/Pt/CIS/FTO	ZP/Ab/Pt/CIS/FTO
1	56.97	37.38	22.72
2	57.53	37.49	22.59
3	57.70	37.21	22.55
Average	57.40	37.36	22.62

### Section 8: Optimization of the immunosensing platform

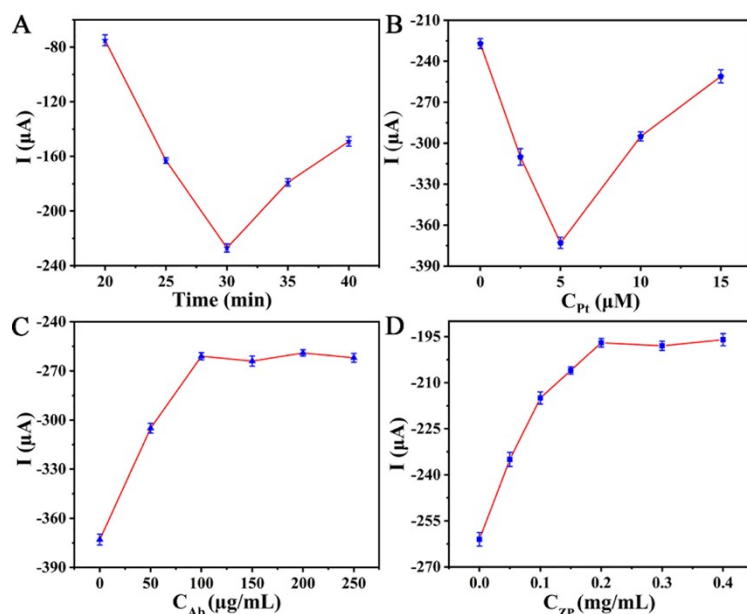
In order to acquire better detection performance, some important conditions for the fabrication of the antifouling biocathode were optimized with the ZIS/FTO photoanode as counter electrode. Fig. S9A shows current response of the CIS/FTO electrode with different electrodeposition times of CIS. With increasing the deposition time to 30 min, the CIS product accumulated moderately on the FTO substrate and the current response enhanced. While with further extension of the deposition time, the current response appeared a gradual decline owing to evident increase of electron diffusion resistance in the extra CIS product. Hence, 30 min of the deposition time for CIS product was adopted.

Fig. S9B presents current response of the Pt/CIS/FTO photocathode decorating with different concentrations of Pt nanoparticles. It was perceived that the concentration of 5  $\mu\text{M}$  for the Pt nanoparticles decoration had an optimal current response. The moderate increase of Pt nanoparticles on the electrode could improve the catalytic activity of the photocathode, while the overloaded Pt nanoparticles inevitably led to electron annihilation by increasing transmission distance to cathodic interface for the photoelectrons.<sup>6</sup>

Fig. S9C displays current response of the Ab-modified photocathode with varied Ab concentrations for incubation. Along with increase in Ab concentration, the current response appeared a gradual decrease at first, and then roughly got a plateau with Ab concentration greater than 100  $\mu\text{g/mL}$ , implying that adequate capture probes were modified on the photocathode. Thus, 100  $\mu\text{g/mL}$  Ab was used as the incubation concentration.

Fig. S9D reveals current response of the antifouling biocathode being incubated with different

concentrations of zwitterionic peptide. As shown, with gradual increase in the concentration of zwitterionic peptide, the current response decreased at first and then came to a platform with the incubation concentration approaching 0.2 mg/mL. Thus, 0.2 mg/mL zwitterionic peptide was selected for preparing the antifouling biocathode.



**Fig. S9.** Current responses of the (A) CIS/FTO electrode with varied deposition times of CIS, (B) Pt/CIS/FTO photocathode with varied concentrations of Pt nanoparticles, (C) Ab-modified photocathode with varied Ab concentrations for incubation, and (D) antifouling biocathode with different concentrations of zwitterionic peptide for incubation.

### Section 9: Antifouling durability of the sensing platform

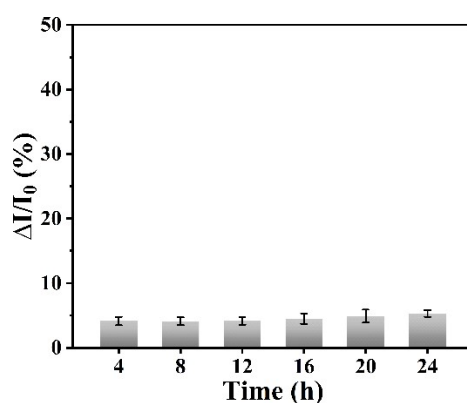


**Fig. S10.** Antifouling durability of the sensing platform with extension of the incubation time in 10% diluted human serum. The signal change ( $\Delta I/I_0$ ) was still below 5% even with the incubation time of 24 h.

## Section 10: Reproducibility, storage stability, and feasibility

The reproducibility of the sensing platform was evaluated by relative standard deviation (RSD) analysis. Through measuring the detection signals of five sensing platforms fabricated separately, the RSD values of 3.5%, 3.2%, and 2.8% were acquired for the probing of 0.1 U/mL, 1 U/mL and 50 U/mL target CA15-3, reflecting a satisfactory reproducibility.

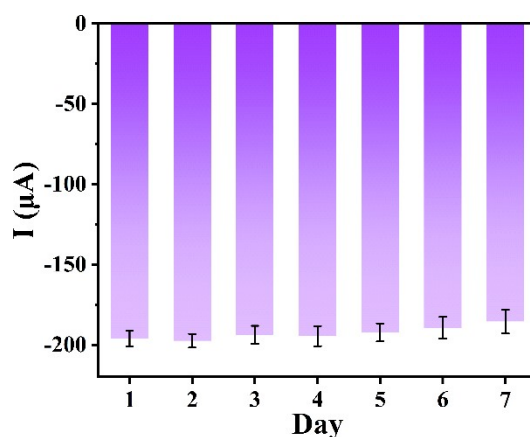


**Fig. S11.** Signal responses of the sensing platform at different storage times. The error bars show standard deviation of five parallel tests.

The storage stability of the sensing platform was inspected by recording the signal responses of five independently prepared platforms every other day, as shown in Fig. S11. After the platforms were stored at 4 °C of a refrigerator for one week, the average signal response still remained 94.1% of the ones freshly prepared, indicating good storage stability.

**Table S2.** Determination of target CA15-3 in human serum samples.

Sample No.	Added (U/mL)	Detected (U/mL) <sup>[a]</sup>	RSD (%)	Recovery (%)
1	1	0.9573	4.0	95.7
2	10	10.65	3.3	106.5
3	50	51.61	3.5	103.2

<sup>[a]</sup> The results were the average of five determinations.

The feasibility of the PEC sensing platform was inspected initially by the recovery experiment in 10-fold diluted serum samples, as exhibited in Table S2. The recoveries were favorably within the scope of

95.7%-106.5%, indicating a promising application against real biological specimens.

## Section 11: References

- [1] S. Peng, P. Zhu, V. Thavasi, S.G. Mhaisalkar, S. Ramakrishna, *Nanoscale*, 2011, **3**, 2602–2608.
- [2] G.W. Wu, S.B. He, H.P. Peng, H.H. Deng, A. L. Liu, X.H. Lin, X.H. Xia, W. Chen, *Anal. Chem.*, 2014, **86**, 10955–10960.
- [3] J. Yuan, P. Wang, C. Hao, G. Yu, *Electrochim. Acta*, 2016, **193**, 1–6.
- [4] Z. Qing, G. Luo, S. Xing, Z. Zou, Y. Lei, J. Liu, R. Yang, *Angew. Chem., Int. Ed.*, 2020, **59**, 14044–14048.
- [5] A.K. Nowinski, F. Sun, A.D. White, A.J. Keefe, S. Jiang, *J. Am. Chem. Soc.*, 2012, **134**, 6000–6005.
- [6] G.C. Fan, S. Gu, D. Zhang, Z. Hu, X. Luo, *Biosens. Bioelectron.*, 2020, **168**, 112563.